Article

Multiple functions integrated inside a single molecule for amplification of photodynamic therapy activity

Xianqing Shi, Qichen Zhan, Yanqing Li, Lin Zhou, and Shaohua Wei

Mol. Pharmaceutics, **Just Accepted Manuscript** • DOI: 10.1021/acs.molpharmaceut.9b00893 • Publication Date (Web): 05 Dec 2019

Multiple functions integrated inside a single molecule for amplification of photodynamic therapy activity

Xianqing Shi[1], Qichen Zhan[1], Yanqing Li[1], Lin Zhou[1]*, Shaohua Wei[1,2]*

[1] College of Chemistry and Materials Science, Jiangsu Key Laboratory of Biofunctional Materials, Jiangsu Collaborative Innovation Centre of Biomedical Functional Materials, Key Laboratory of Applied Photochemistry, Nanjing Normal University, Nanjing, Jiangsu 210023, China.

[2] School of Chemistry and Chemical Engineering, Yancheng Institute of Technology, Yancheng, Jiangsu 224051, China.

E-mail: zhoulin@njnu.edu.cn (L. Zhou), shwei@njnu.edu.cn (S.H. Wei).

X.Q. Shi and Q.C. Zhan contributed equally to the work.

ABSTRACT: Nitric oxide (NO) can play both pro-survival and pro-death roles in photodynamic therapy (PDT). The generation efficiency of peroxynitrite anions ($ONOO^-$), by NO and superoxide anions ($O_2^{\bullet -}$), significantly influenced the outcome. Reports indicated that such efficiency is closely related to the distance between NO and $O_2^{\bullet -}$. Thus, in this manuscript, L-arginine (Arg) ethyl ester modified zinc phthalocyanine (Arg-ZnPc) was designed and synthesized as a photosensitizer (PS) and NO donor. Post light irradiation, the guanido of Arg-ZnPc can be effectively oxidized by the generated reactive oxygen species (ROS) in PDT process to release NO. Such strategy could ensure $O_2^{\bullet -}$ and NO generation in the same place at the same time to guarantee the effective $ONOO^-$ formation. In addition, NO has other multiple synergistic cancer treatment functions, including tumor tissue vasodilatation for drug extravasation promotion, P-glycoprotein (P-gp) down-regulation for drug efflux inhibition and glutathione (GSH) depletion for cancer cell endogenous anti-oxidant defense destruction. In vitro and in vivo results indicated that the effective $ONOO^-$ formation and multiple functions of Arg-ZnPc could synergistically enhance its PDT activity and ensure its satisfactory cancer treatment outcome.

Keywords: Zinc phthalocyanine; nitric oxide; photodynamic therapy; synergistic treatment.

INTRODUCTION

PDT utilizes non-toxic PS, light and O_2 to generate cytotoxic ROS, including singlet oxygen ($^1O_2$), $O_2^{\bullet -}$, hydroxyl radicals ($HO^{\bullet}$), hydrogen peroxide (H_2O_2), et al, to kill cancer. [1] PDT has been authorized by the U.S. food and drug administration for oncotherapy because of its low system toxicity and slight trauma. [2]

In recent years, gas, such as NO, [3] CO, [4] SO_2, [5] H_2S, [6] et al., attracted great attention in disease treatment. Under normal physiological condition, above gases are necessary physiological messengers with important biological function and negligible toxicity. However, elevated concentrations of these gases can kill cancer cells directly. [5] And they also can play synergistic tumor suppression function with other treatment modality, such as chemotherapy, photothermal therapy, et al. [3, 7] Using these gases to influence diverse physiological and pathophysiological processes for direct or assistant disease treatment was denoted as gas therapy. [8]

NO is a gaseous molecular messenger among the gas transmitter family. Several of its functions, such as down-regulating P-gp expression to inhibit drug efflux, [9] reacting with $O_2^{\bullet -}$ to generate high biocidal $ONOO^-$, [10] promoting vasodilatation to enhance drug tumor accumulation [11] and damaging GSH to break anti-oxidant defense, [12] are beneficial to tumor therapy in PDT. However, different researches indicated that NO could play both negative (pro-survival) [13-16] and positive (pro-death) [17-19] roles in PDT treatment. [20] These controversial results closely related to PDT dose [19] and NO treatment timing, location or concentration. [21]

In addition, the generation efficiency of $ONOO^-$, a reactive nitrogen species (RNS) formed by $O_2^{\bullet -}$ and NO, [21] is the predominant pro-cell death mechanism in NO treatment on account of its high oxidative damage activity. However, if the distance between $O_2^{\bullet -}$ and NO source is not close enough, $ONOO^-$ formation efficiency would be ultra-low. [22] In addition, the half-life time of NO is extremely short (~ 1 s) and it is rapidly converted into nitrate by oxyhemoglobin in blood. [23] Therefore, it is significant to control the release of NO inside tumor cells. Co-loading PS and NO donor (with tumor microenvironment or ROS response release function) inside one nanoscale carrier is a classical way to meet the above requirements. [24-27] As an alternative option, integration ROS responsive NO donor within PS could be an ideal method to utilize NO

in PDT process because such strategy could ensure $O_2^{\bullet-}$ and NO generation in the same place at the same time to guarantee the effective $ONOO^-$ formation.

Guanido of arginine could be oxidized by ROS to release NO. [28] Thus, in this manuscript, L-arginine ethyl ester modified ZnPc (Arg-ZnPc) was designed and synthesized as a PS with ROS responsive NO donor. As shown in Scheme 1, post trapping by cancer cells and irradiating by light, Arg-ZnPc could generate abundant ROS (including $O_2^{\bullet-}$) to play PDT activity and trigger NO release in the same place at the same time. Thus, the effective $ONOO^-$ generation could guarantee the synergistic oxidative damage of ROS and RNS. Furthermore, NO could promote tumor vasodilatation and down-regulate cancer cells P-gp expression to enhance drug extravasation and retention at tumor tissue. Reduced GSH builds endogenous anti-oxidant defense inside cells. [29] And many recent researches indicated that the high concentrations of reduced GSH in cancer cells could consume ROS to reduce PDT activity. [30-32] NO could deplete GSH to avoid ROS or RNS nontherapeutic consumption and further enhance their oxidative damage efficiency. Furthermore, L-lysine (Lys) ethyl ester modified ZnPc (Lys-ZnPc), with similar structure to Arg-ZnPc but without guanido, was synthesized as a control drug to prove the released NO from guanido of Arg-ZnPc dominated above synergistic functions. All researches indicated that integration ROS responsive NO donor within PS was an ideal method to utilize NO in PDT process.

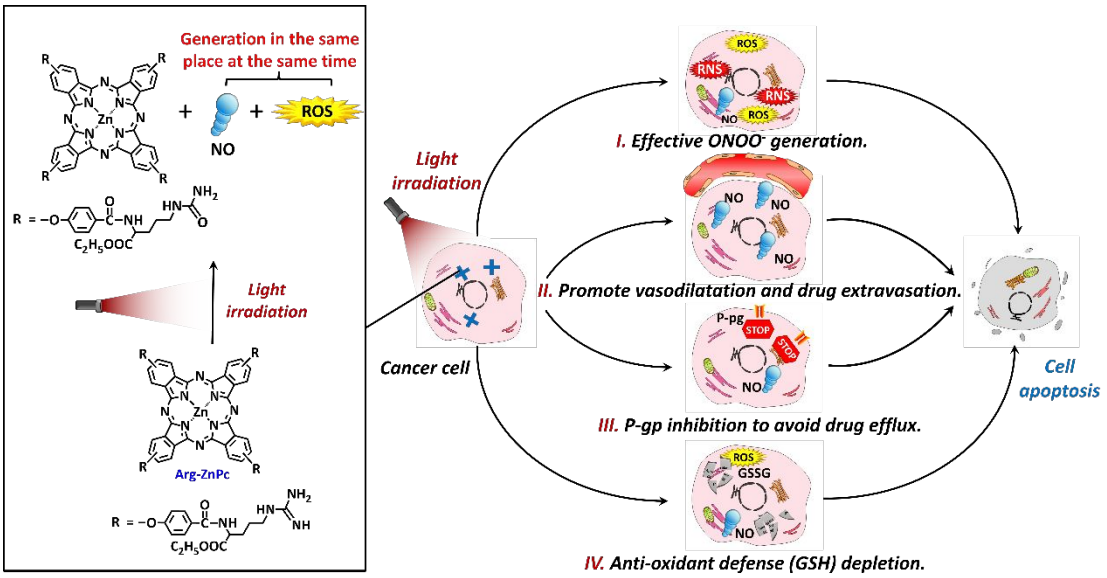

Scheme 1. Mechanism diagram of multiple functions integrated inside Arg-ZnPc for its PDT activity amplification (I: NO and react with $O_2^{\bullet-}$ to regenerate $ONOO^-$ to kill cancer cells directly;

II: tumor tissue vasodilatation can promote PS extravasation to enhance its accumulation at tumor tissue; III: P-gp down-regulation can inhibit intracellular PS efflux to elevate its concentration inside cancer cells; IV: GSH depletion destroy cancer cell endogenous anti-oxidant defense to avoid ROS consumption).

EXPERIMENT SECTION

Synthesis of Arg-ZnPc, Lys-ZnPc and Two-photon-excitable and NIR-emissive Fluorescence Probe (TPNIR-FP). The synthetic routes of Arg-ZnPc and Lys-ZnPc were shown in Scheme 2. Synthesis of TPNIR-FP was shown in Scheme 3. These compounds were identified by infrared absorption spectra (IR), ^{1}H NMR spectra, ^{13}C NMR spectra and Mass spectra (MS) spectrometer.

Synthesis of ZnPc. The 4-(3, 4-dicyanophenoxy) benzoic acid was synthesized according to our previous report. [33] Then above product (586.3 mg, 2.22 mmol) and $Zn(OAc)_2$ (241.7 mg, 1.32 mmol) were dissolved in 1-pentanol (8 mL). Under the protection of N_2, the reaction temperature was heated to 90 °C for 1 h. Later, 1, 8-Diazabicyclo [5, 4, 0] undec-7-ene (DBU, 300 μL) was added and the temperature continued heating to 140 °C for reacting 12 h. Later, when cooled down to room temperature, residual 1-pentanol was dislodged via vacuum distillation. Then crude green product was treated via column chromatography, and ethyl acetate/methyl alcohol = 1/3 and DMF/alkaline water = 2/1 (v/v) were chosen as developing solvent, successively. The ZnPc could precipitate out by adjusting pH = 4, and then, dissolved in alkali water to remove insoluble impurities. The green product was treated with distilled water and acetone several times. Finally, pure product was received after vacuum dried (113.8 mg, 18.3%). M. P. > 200 °C. IR (KBr, cm^{-1}): 3460, 1700 (C = O), 1603, 1467, 1401, 1236, 1163. ^{1}H NMR (400 MHz, d_6-DMSO): δ (ppm) 8.88 (br, 4H, Pc-H), 8.49 (br, 4H, Pc-H), 8.22-8.11 (m, 8H, Ar-H), 7.83-7.78 (m, 4H, Pc-H), 7.58-7.48 (m, 8H, Ar-H). ^{13}C NMR (100 MHz, d_6-DMSO): δ (ppm) 167.41, 161.48, 157.30, 151.35, 139.70, 133.87, 132.41, 126.87, 124.29, 121.40, 118.81, 118.30, 1112.63. MS-MALDI-TOF (m/z): calcd for $C_{60}H_{32}N_8O_{12}Zn$: 1122.3. Found $[M + H]^+$ 1122.3.

Synthesis of Arg-ZnPc and Lys-ZnPc. ZnPc (52.7 mg, 46.96 μmol), 1-(3-Dimethylaminopropyl)-3-ethylcarbodiimide hydrochloride (EDC·HCl, 68.3 mg, 356.40 μmol) and 1-Hydroxybenzotriazole (HOBt, 51.1 mg, 378.20 μmol) were added into 6 mL N, N-Dimethylformamide (DMF) and kept reacting for 1 h at 20 °C. In the ice-water bath, above mixture was dropped into the L-Arginine ethyl ester hydrochloride (105.4 mg, 383.02 μmol) and N, N-Diisopropylethylamine (DIPEA, 0.5 mL, 3.02 mmol) solution (4 mL DMF). After then, the reaction was kept for another 1 h at 0 °C. Next, the mixture was added into CH_2Cl_2 (60 mL) and the sediment was collected via centrifugation. The crude solid was dissolved in acidic aqueous solution (pH = 4). After centrifugation, the supernatant was obtained, and adjusted pH to 10 by 10% (wt%) NaOH. The solid product was purified via centrifugation again, then rinsed with ethyl acetate several times. Then, Arg-ZnPc (21.4 mg, 25.8 %) was afforded by vacuum drying. M. P. > 200 °C. IR (KBr, cm^{-1}): 3361, 1733 (ROC = O), 1646 (C = O), 1484, 1229, 1093. ^1H NMR (400 MHz, d_6-DMSO): δ (ppm) 9.23 (dd, 4H, J_1 = 6.92 Hz, J_2 = 16.08 Hz, CONH), 8.95-8.80 (m, 8H, H of guanidino), 8.17-7.79 (m, 16H, Pc-H, Ar-H), 7.52-7.41 (m, 12H, Pc-H, Ar-H), 4.47 (s, 4H, CH), 4.16 (t, 8H, J = 6.68 Hz, CH_2), 3.17 (s, 8H, CH_2), 1.89 (s, 8H, CH_2), 1.66 (s, 8H, CH_2), 1.25-1.16 (m, 12H, CH_3). MS-MALDI-TOF (m/z): calcd for $C_{92}H_{96}N_{24}O_{16}Zn$: 1859.28. Found: $[M + H]^+$ 1859.30.

The synthesis of Lys-ZnPc was similar to Arg-ZnPc. M. P. > 200 °C. IR (KBr, cm^{-1}): 3414, 1726 (ROC=O), 1639 (C=O), 1480, 1236, 1083. ^1H NMR (400 MHz, d_6-DMSO): δ (ppm) 8.66-8.46 (m, 8H, Ar-H), 8.27-8.08 (m, 8H, Pc-H), 8.05-7.95 (m, 4H, Pc-H), 7.59-7.46 (m, 4H, Ar-H), 7.42-7.27 (m, 4H, Ar-H), 4.53 (s, 4H, CH), 4.14-4.10 (m, 8H, CH_2), 1.85 (s, 8H, CH_2), 1.57 (s, 8H, CH_2), 1.26-1.16 (m, 20H, CH_2, CH_3). MS-MALDI-TOF (m/z): calcd for $C_{92}H_{96}N_{16}O_{16}Zn$: 1747.2. Found: $[M + H]^+$ 1747.2.

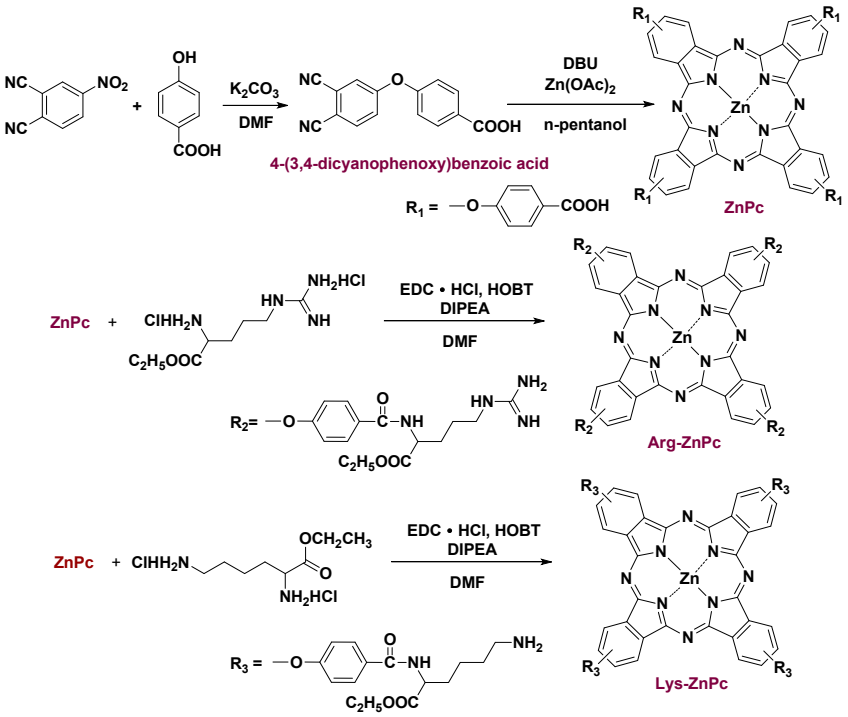

Scheme 2. Synthesis route of ZnPc derivatives.

Synthesis of TPNIR-FP. Two-photon-excitable and NIR-emissive amidogen (TPNIR-NH_2) was synthesized according to previous literature. [34] TPNIR-FP was used to detect $ONOO^-$ and it was also synthesized according to previous literature. [35]

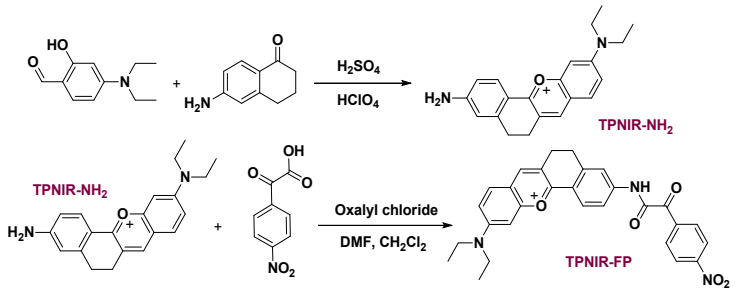

Scheme 3. Synthetic routes of TPNIR-FP.

Cell and Animals. Murine mammary carcinoma (4T1) and human cervical carcinoma (Hela) cells were bought from the Cell Bank of Chinese Academy of Science (Shanghai, China). The cells were incubated in Dulbecco's modified eagle medium (DMEM) with 10% (v/v) fetal bovine serum FBS in the incubator (5 % CO_2, 37 °C). All animals were purchased from Yangzhou University, the center for comparative medicine. The animal experiments were conducted according to the Guide for the Care and Use of Laboratory Animals, which was the

guidelines of Nanjing Normal University.

Analysis of Anticancer Activity in Vitro. 3-(4, 5-dimethylthiazol-2-yl)-2, 5-diphenyltetrazolium bromide (MTT) colorimetric assay was used to detect the dark and light cytotoxicity, Hela cells were incubated on 96-well plates for 24 h. Arg-ZnPc or Lys-ZnPc was treated with the concentration ranging from 0 to 10 μM for incubating in dark condition. Besides, the drugs with the concentration of 2 μM were added inside cells respectively. After 48 h, the cells were in dark or irradiated under 665 nm light emitting diode (LED, 5 W, light dose for in vitro experiment was 0.4 W/cm^2) for 4 min. Next, the cell survival ability was detected with MTT assay using microplate reader.

Cell cytotoxicity behaviors of Arg-ZnPc and Lys-ZnPc were also studied by flow cytometry (FCM), respectively. The cells, treated with Arg-ZnPc or Lys-ZnPc, were illuminated by light for 4 min. After incubating for 24 h, the apoptosis properties were detected using the apoptosis assays kit (Annexin V/FITC-PI). Besides, the Hoechst 33342, which the concentration was 25 μg mL^{-1} in DMEM, was put into the irradiated cells and cultured in dark for another 0.5 h. Then, blue fluorescence in above cells was observed with the confocal laser scanning microscopy (CLSM, 405 nm laser, 100 mW, 5% strength).

In Vivo Anticancer Activity. The BALB/c mice (female, ~20 g) bearing tumor model was built via hypodermic injection with 4T1 cells. These mice were grouped 3 teams randomly when the tumor size was reached about 100 mm^3. Then the mice were intravenously injected with saline, Arg-ZnPc or Lys-ZnPc (the dosage of drugs was 2 mg kg^{-1}), respectively. Then, tumor sizes of mice were recorded every day with dark condition or irradiated by 665 nm LED (5 W, light dose for in vivo experiment was 0.9 W/cm^2) for 30 min. The tumor length (L), width (W) and the weight of mice were recorded during the treatment. Then the above mice were sacrificed after 14 days and dissected to obtain the main organs, which included heart, liver, spleen, lung, kidney and brain. The calculation formula of tumor volume (V) was: V (mm^3) = $L \times W^2 / 2$. And the tumor suppression effect of the two ZnPc was evaluated by comparing their V_t/V_0 value during 14 days' treatment (V_t: represented the tumor volume post t days treatment; V_0: represented tumor volume at day 0)

ROS and RNS Detection in PDT Process. The fluorescence intensity of ROS and reactive nitrogen species (RNS) could be detected via chemical process with 9, 10-anthracenedip-ropionic acid (ADPA), dihydroethidium (DHE), 3-Amino, 4-aminomethyl-2′, 7′-difluorescein, diacetate (DAF-FM DA) and TPNIR-FP as the probe to monitor the fluorescence changes. Extracellular $^1O_2$ generation was detected by ADPA. The interaction between ADPA and $^1O_2$ could produce its endoperoxide, inducing the decrease of its absorbance intensity (the λ_{max} of ADPA was 378 nm). 18 μL ADPA (6 mM) was mixed with 3 mL aqueous of Arg-ZnPc or Lys-ZnPc. Immediately, the above samples were irradiated with a 665 nm irradiation. The above spectra were recorded from 0 to 3 min.

Then, the formation of NO was detected with DAF-FM DA test kits. 3 μL of DAF-FM DA in DMSO was hydrolyzed to DAF-FM by 0.01 M NaOH (3 mL) for 20 min at room temperature. And the reaction was stopped with 3 mL phosphate buffered saline. DAF-FM (2.5 μM) was mixed with aqueous of Arg-ZnPc or Lys-ZnPc. The fluorescence intensity was detected from 0 to 54 min, which the excitation wavelength was 495 nm. The fluorescence changes of superoxide anions and $ONOO^-$ with time were measured respectively.

Besides, DHE or TPNIR-FP were mixed with aqueous solution, respectively. Then the drugs of Arg-ZnPc or Lys-ZnPc were put into the solution. Immediately, the solution was irradiated by light with different time (DHE: from 0 to 6 min; TPNIR-FP: from 0 to 12 min).

The corresponding ROS and RNS probes, including singlet oxygen sensor green reagent (SOSG), DHE, DAF-FM DA, TPNIR-FP, 2' 7'-Dichlorofluorescin diacetate (DCFH-DA), were served to monitor $^1O_2$, $O_2^{\bullet -}$, NO, $ONOO^-$ and H_2O_2 generation in cells post treating by drugs and light. Cells were cultured in confocal dishes and treated with drugs (2 μM). After 48 h and the samples were irradiated by light for 4 min, the probes (5 μM) as an indicator were added into the dishes for 1 h. Then washing cells with phosphate buffered saline, the fluorescence inside cells was observed via CLSM. The parameter settings of CLSM for ROS/RNS detection were listed as follows: (1) For $^1O_2$ detection using SOSG: 488 nm laser, 150 mW, 15% strength; (2) For $O_2^{\bullet -}$ detection using DHE: 561 nm laser, 150 mW, 10% strength; (3) For NO detection using DAF-FM DA: 488 nm laser, 15% strength; (4) For $ONOO^-$ detection using TPNIR-FP: 561 nm laser, 150 mW, 5% strength; (5) For ROS/RNS detection using DCFH-DA: 488 nm laser, 150 mW, 15% strength.

Besides, the NO, ROS and RNS generation in cells using their specific scavengers. Carboxy-PTIO (c-PTIO), ADPA, tempol and L-cysteine were selected as the scavenger of NO $^1O_2$, $O_2^{\bullet -}$ and $ONOO^-$, respectively. Briefly, c-PTIO (100 μM), ADPA (500 μM), tempol (1500 μM) or L-cysteine (500 μM) was added in cells for incubation 1 h in advance. Then Arg-ZnPc was treated and their corresponding probes were added as described above, respectively, while the other sample was directly treated Arg-ZnPc to compare their fluorescence intensity.

Detection of GSH Content in Vitro. GSH content was measured by GSH and oxidized glutathione (GSSG) assay kit. Briefly, the preparation of total glutathione content was tested as follows. Cells were cultured in 6-well plates and treated by Arg-ZnPc or Lys-ZnPc. Then the one kind of above samples were incubated in dark and another incubated with 4 min light irradiation. After that, the cells were washed and centrifuged. After removing the supernatant, the protein removal reagent was added and vortexed sufficiently, which the content was three times than the cells volume. The samples were frozen and thawed twice by liquid nitrogen and 37 °C water bath, and placed in 4 °C for 5 min. After that, the samples were centrifuged at 10000 g (4 °C) for 10 min. The obtained supernatant was used for the determination of total glutathione. The preparation of GSSG content was detected as follows. Part of the above samples were added into the diluted GSH scavenging auxiliary solution at the rate of 20 μL per 100 μL, then vortex immediately. GSH scavenging working fluid was added at the rate of 4 μL per 100 μL, then vortex immediately and reacted at 25 °C for 60 min. The above treatment could be used for the measurement of GSH levels.

Besides, GSH probe was synthesized to detect the GSH levels in cells. Cells were incubated in confocal dishes and treated with different drugs. After 4 min light irradiation, GSH probe (5 μM) was added and the green fluorescence was observed by CLSM (488 nm laser, 150 mW, 5% strength) after 30 min incubation.

P-gp Expression and Uptake of Drugs in Vitro. P-gp expression was quantified by western blot assay. Cells were cultured in 6-well plates and treated by Arg-ZnPc or Lys-ZnPc. After 48 h, the cells were irradiated by light for 4 min and incubated for another 4 h. Later, the cells were lysed by radio immune precipitation assay (RIPA) and collected after centrifugation to obtain the total protein. Also, the protein quantification was detected by bicinchoninc acid

protein assay reagent. The protein samples were resolved using sodium dodecyl sulfate polyacrylamide gel electrophoresis. Next, the above samples were transferred to polyvinylidene fluoride membrane, and ponceaux was used to stain them for about 1 min and washed by tris-buffered saline with Tween (TBST). After that, the membranes were sealed using 5% nonfat milk and incubated with antibodies of P-gp (1:500) and glyceraldehyde-3-phosphate dehydrogenase (GAPDH) (0.8:3000) at 4 °C. Overnight, the secondary antibody was added for incubating at room temperature. P-gp protein was detected by enhanced chemiluminescence system (ECL).

Cells were cultured in confocal dishes and the drugs were treated for incubating different time, including 8 h, 48 h, 72 h and 96 h, and red fluorescence was observed with CLSM (647 nm laser, 200 mW, 10% strength). Meanwhile, cell uptake amount could be calculated by UV-Vis spectrum. After seeded cells in 24-well plates, the Arg-ZnPc or Lys-ZnPc was treated and incubated another 8 h, 24h, 45h, 48 h, 72 h and 96 h using colorless DMEM with 1% FBS. Then the supernatant was removed and measured the UV absorbance value.

Fluorescence Imaging and Enhanced Permeability and Retention in Vivo. The BALB/c mice bearing tumor model were established by subcutaneous injection using 4T1 cells. 2 mg kg^{-1} of drugs were administrated by intravenous injection three times and the above mice were sacrificed, dissected them to achieve visceral organs, including heart, liver, spleen, lung and kidney, and tumors for the fluorescence imaging.

Evans blue assay was used to verify the NO generation inducing the enhancement of vascular permeability. 10 mg kg^{-1} of evans blue was intravenous injected to the mice. Immediately the drugs were subcutaneous and intravenous injected (2 mg kg^{-1} of drugs have been treatment for 3 days) to the mice and irradiated for 10 min. After 2 h, the mice were dissected for obtaining the target skin and tumor, then the above skin and tumor were immersed with methanamide (100 mg mL^{-1}) in 60 °C for 24 h so as to detect the value of the evans blue extravasation at the 470 nm absorbance.

The Analysis of Data. The statistical analysis was performed by ANOVA and the value of $p<0.05$ was considered meaningful. The value of $^{*}p<0.05$, $^{**}p<0.01$ and $^{***}p<0.001$ were the drugs treated groups versus control and the value of $^{\#}p<0.05$, $^{\#\#}p<0.01$ and $^{\#\#\#}p<0.001$ were

Lys-ZnPc treated group versus Arg-ZnPc treated group.

RESULTS AND DISCUSSION

Synthesis and Characterization of Arg-ZnPc and Lys-ZnPc. To prove the released NO from guanido of Arg-ZnPc guarantee the synergistic anticancer effect, Lys-ZnPc, with similar structure to Arg-ZnPc but without guanido, was synthesized and its PDT activity was studied and compared with Arg-ZnPc. A mixture of four possible structural isomers, C_{4h}, C_{2v}, C_s, and D_{2h}, is obtained from the synthesis of tetra-substituted phthalocyanines. [36] However, the isomers are difficult to separate. [37] But, generally, C_{4h} is the major isomer. [38-40] In this study, Arg-ZnPc and Lys-ZnPc were obtained as isomer mixtures. But Arg-ZnPc and Lys-ZnPc are modified from a tetra-carboxyl substituted ZnPc. Thus, we proposed that they could have similar isomer form ratio. The chemical structure (C_{4h} isomer form) of Arg-ZnPc and Lys-ZnPc were presented in Figure 1A and Figure S1. Furthermore, Arg-ZnPc and Lys-ZnPc were verified by IR, ^{1}H NMR spectra, and MS spectrometer. The molar extinction coefficients of Arg-ZnPc and Lys-ZnPc at various wavelength ($\varepsilon_{monomer}$, $\varepsilon_{aggregator}$ and $\varepsilon_{665nm\ of\ light\ source}$) via the Lambert-Beer law were listed in Table S1 and Figure S2.

In Vitro Anticancer Activity. In vitro toxicity of ZnPcs were assessed by MTT assay. Without light irradiation, the two ZnPcs showed weak toxicity in cancer cells at low concentration (< 4 μM, Figure S3). Thus, we chose the drug concertation of 2 μM for further phototoxicity and in vitro anticancer mechanism analysis to avoid their dark toxicity influence. However, after light irradiation, the viability of Arg-ZnPc (2 μM) treated cells rapidly decreased but the viability of Lys-ZnPc (2 μM) treated cells only showed slightly decreased (Figure 1B).

In addition, the cancer cell apoptosis by the two ZnPcs post light irradiation were studied by FCM assay. [41] The apoptotic cells percent (Q2 and Q3 zones) in Arg-ZnPc treated cells post light irradiation was about 66.9%. However, only 11.0% of apoptotic cells could be observed in Lys-ZnPc treated cells post same treatment (Figure 1C and 1D).

The nuclei of the cells could be stained for DNA with Hoechst 33342 dye with blue fluorescence signal. [42] The fluorescent signal in control cells for Hoechst 33342 were dimmed with uniform distribution pattern. In apoptotic cells, their DNA condensed and their Hoechst

33342 signal should be bright with concentrated distribution pattern. Thus, apoptosis induced nuclear condensation can therefore be used to distinguish Hoechst 33342 signal changes. As shown in Figure 1E and Figure S4, DNA condensing degree of Arg-ZnPc group was more significant comparing with Lys-ZnPc group post light irradiation. All of above data proved the superior light cytotoxicity of Arg-ZnPc rather than Lys-ZnPc.

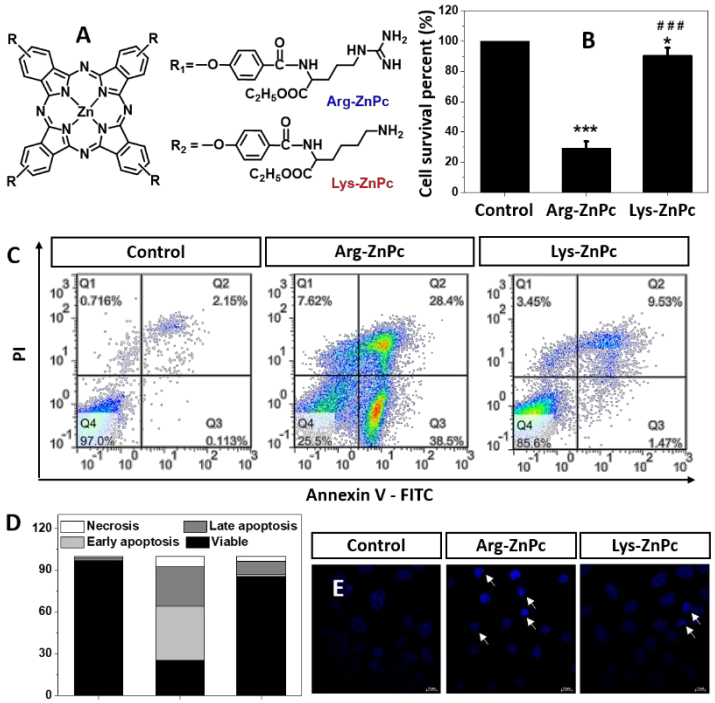

Figure 1. The chemical structure of Arg-ZnPc and Lys-ZnPc (A, only the major C_{4h} isomer is shown for Arg-ZnPc and Lys-ZnPc, which likely contains other isomers); light toxicity comparison of Arg-ZnPc and Lys-ZnPc post 665 nm light irradiation (B); cell apoptosis by Arg-ZnPc and Lys-ZnPc by FCM assay (C) and their relative events percent comparison (D); Hoechst 33342 staining pattern in control, Arg-ZnPc and Lys-ZnPc post light irradiation (E).

In Vivo Antitumor Activity. As shown in above in vitro results, without light irradiation, the toxicity of Arg-ZnPc and Lys-ZnPc were very weak, which could be sure their safety in vivo treatment. However, after irradiating the PS accumulated tumor tissue, they could show tumor suppression effect. To verify this hypothesis and compare the safety in vivo and tumor suppression activity of Arg-ZnPc and Lys-ZnPc, bilateral subcutaneous transplantation tumor model was used.

As shown in Figure 2A, during 14 days' treatment, no significant weight loss in all groups. And the obvious pathological changes were detected in main organs slices by Hematoxylin & eosin (H&E) stain method (Figure 2B) (purple hematoxylin label nucleic acids and pink eosin label inside and outside cell proteins [43]) after 14 days' treatment. These results proved the good safety of the two ZnPcs.

During 14 days' treatment by Arg-ZnPc or Lys-ZnPc and light irradiation at tumor site, their tumor volumes were recorded every day. As shown in Figure 2C, both Arg-ZnPc and Lys-ZnPc could suppress tumor growth in comparison with the control mice. And treatment outcome of Arg-ZnPc group was superior to Lys-ZnPc one. Besides, as shown in Figure S5, no obvious tumor suppression effect was detected in Arg-ZnPc or Lys-ZnPc treated mice without light irradiation. In addition, serious nuclear damage was detected in Arg-ZnPc group, which further proved the effective tumor cell death post treatment (Figure 2D).

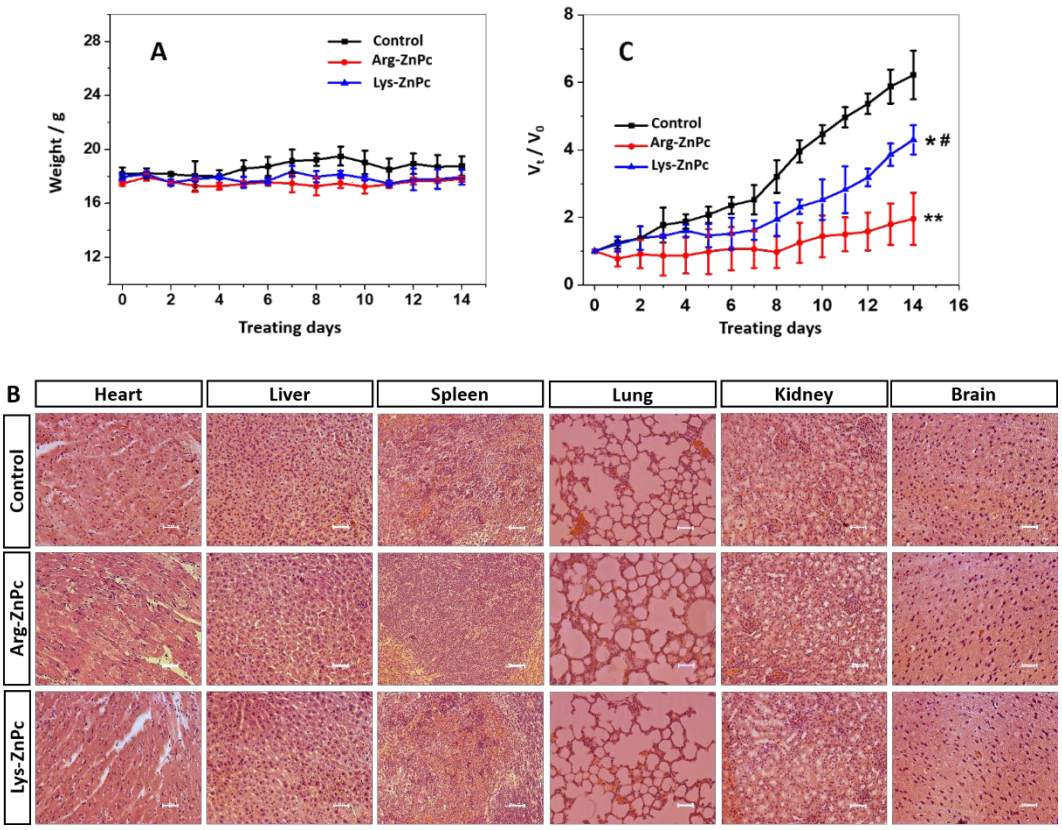

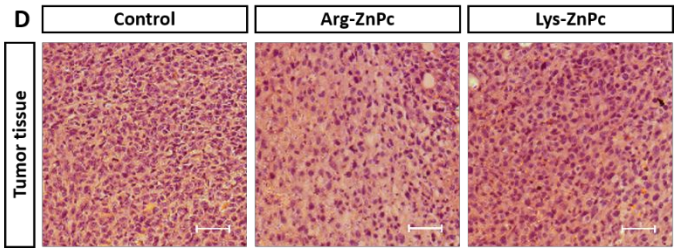

Figure 2. The weight (A) and relative tumor volume (C) changes of the mice during 14 days' treatment by various drugs and light irradiation at tumor tissue; H&E labeled main organs (B) and tumor tissue (D) sections post 14 days' treatment (Bar = 50 μm).

Synergistic Anticancer Mechanism of Arg-ZnPc

RNS Synergistic Effect with ROS Based on NO Generation by Arg-ZnPc. $^1O_2$ is a predominant ROS in PDT. $O_2^{\bullet-}$ and NO are key factors for $ONOO^-$ generation. Thus, extracellular $^1O_2$, $O_2^{\bullet-}$, NO and $ONOO^-$ formation by Arg-ZnPc and Lys-ZnPc were studied using ADPA, DHE, DAF-FM and TPNIR-FP probes by spectra method, separately.

ADPA would convert to its endoperoxide by $^1O_2$, which could induce its absorbance intensity decreasing. Figure 3A showed the decrease in absorbance intensity of ADPA by Arg-ZnPc or Lys-ZnPc, as a function of light exposure time, indicating their effective $^1O_2$ generation post light irradiation. The decrease degree of Arg-ZnPc was higher than that of Lys-ZnPc, indicating that the $^1O_2$ production capability of Arg-ZnPc was stronger than Lys-ZnPc.

DHE reacts with $O_2^{\bullet-}$ to form a fluorescent product ethidium. As shown in Figure 3B, both Arg-ZnPc and Lys-ZnPc could induce DHE fluorescence intensity enhancing, indicating their effective $O_2^{\bullet-}$ generation post light irradiation.

The guanido of Arg-ZnPc can effectively release NO via oxidization by ROS in PDT process. DAF-FM could interact with NO to generate benzotriazole derivative with strong fluorescence. [44] It was observed that the fluorescence was significantly enhanced post the treatment of Arg-ZnPc (Figure 3C) and light irradiation, indicating NO release. On the contrary, no NO generation could be detected in Lys-ZnPc treated group.

$O_2^{\bullet-}$ could react with NO to generate $ONOO^-$, a RNS with higher biocidal activity than ROS.[18] According to previous reports, TPNIR-FP could react $ONOO^-$ to generate a product (TPNIR-NH_2) with strong red fluorescence. Thus, TPNIR-FP was used to detected $ONOO^-$

generation post light irradiation. As obviously observed in Figure 3D, the Arg-ZnPc could effectively generate the $ONOO^-$.

Many researchers suggested that these isomers have similar physical and chemical properties. [45, 46] And some researches indicated that the isomers of some phthalocyanines could have different UV-visible absorption property, such as different monomer/aggregator peak position, strength and ratio, which could influence their ROS generation ability and PDT activity. [47-49] As shown in Figure S2, the monomer and aggregator peak for Arg-ZnPc and Lys-ZnPc were similar but their monomer/aggregator peak strength and ratio were different. The monomer form of ZnPc was more conducive for ROS generation. Even if Lys-ZnPc has more monomer than Arg-ZnPc, the ROS production capability of Lys-ZnPc was lower than that of Arg-ZnPc. Thus, the ROS generation capability enhancement of Arg-ZnPc comparing with Lys-ZnPc was not due to its aggregation states and isomers existence.

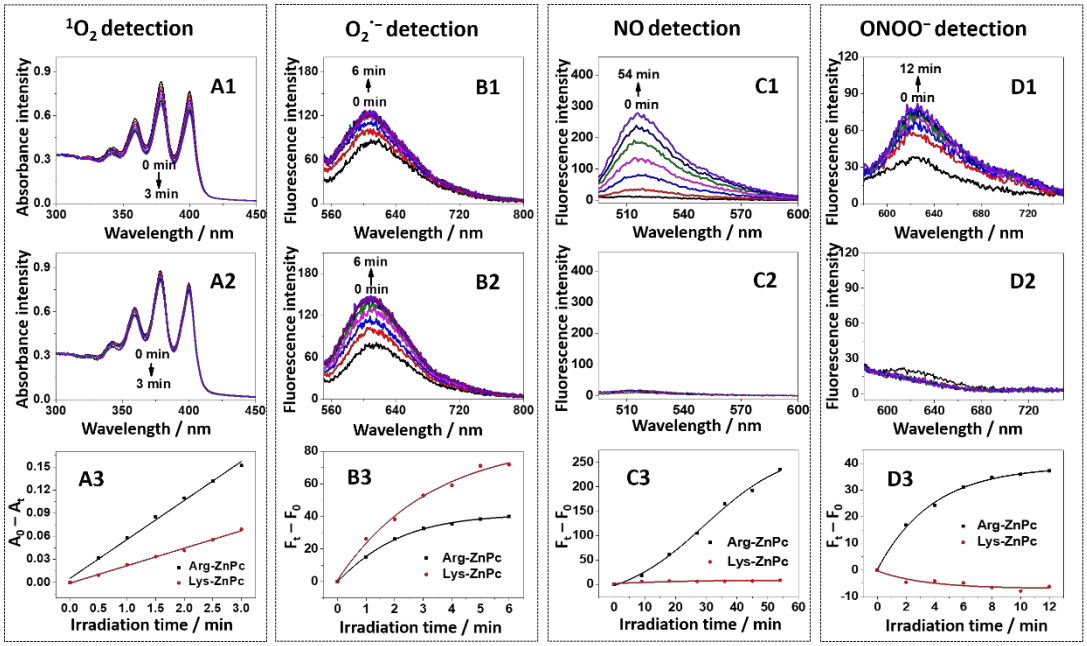

Figure 3. (A) $^1O_2$ probe bleaching effect by Arg-ZnPc (A1) and Lys-ZnPc (A2) post light irradiation, and (A3) absorbance intensity change degree as a function of irradiation time (A_0 means the absorbance intensity at the 0 min and A_t means the absorbance intensity at the other time); (B) $O_2^{\bullet-}$ probe fluorescence enhancing effect by Arg-ZnPc (B1) and Lys-ZnPc (B2) post light irradiation, and (B3) fluorescence intensity change degree as a function of irradiation time (F_0 means the fluorescence intensity at the 0 min and F_t means the fluorescence intensity

at the other time); (C) NO probe fluorescence enhancing effect by Arg-ZnPc (C1) and Lys-ZnPc (C2) post light irradiation, and (C3) fluorescence intensity change degree as a function of irradiation time; (D) $ONOO^-$ probe fluorescence enhancing effect by Arg-ZnPc (D1) and Lys-ZnPc (D2) post light irradiation, and (D3) fluorescence intensity change degree as a function of irradiation time.

In addition, intracellular $^1O_2$, $O_2^{\bullet -}$, NO, $ONOO^-$ and ROS+RNS were detected by SOSG, DHE, DAF-FM DA, TPNIR-FP and DCFH-DA probes using CLSM (Figure 4 and Figure S6-S10). And most the intracellular detection obtained similar results as above extracellular detection. However, Arg-ZnPc is more efficient in $^1O_2$ generation but less efficient in $O_2^{\bullet -}$ generation than Lys-ZnPc in aqueous solution. In contrast, for ROS detection inside cancer cells, Arg-ZnPc is more efficient in $^1O_2$ and $O_2^{\bullet -}$ generation than Lys-ZnPc possibly because of the difference between pure water and complicated cytoplasm. DCFH-DA could response to both ROS and RNS to generate fluorescent DCF. [50] And Arg-ZnPc has higher total ROS and RNS production ability than Lys-ZnPc to ensure its ROS-RNS synergistic oxidative damage.

Furthermore, under our experiment condition for ROS/RNS detection (drug incubation time was 48 h), there were no obvious difference of cellular uptake efficiency between Arg-ZnPc (the uptake percent was 88.76% ± 2.84%) and Lys-ZnPc (the uptake percent was 86.74% ± 7.75%) (Figure S11). Thus, the ROS/RNS generation differences between Arg-ZnPc and Lys-ZnPc is due to the compound, but not the variability in cellular uptake. In addition, the NO, ROS and RNS generation experiments were validated using their specific quenchers. c-PTIO (Figure S12), ADPA (Figure S13), tempol (Figure S14) and L-cysteine (Figure S15) were selected as the scavenger of NO, $^1O_2$, $O_2^{\bullet -}$ and $ONOO^-$, respectively. The NO, ROS and RNS probes fluorescence intensity by Arg-ZnPc treated alone was higher than adding their corresponding scavengers, which further validated NO, ROS and RNS generation.

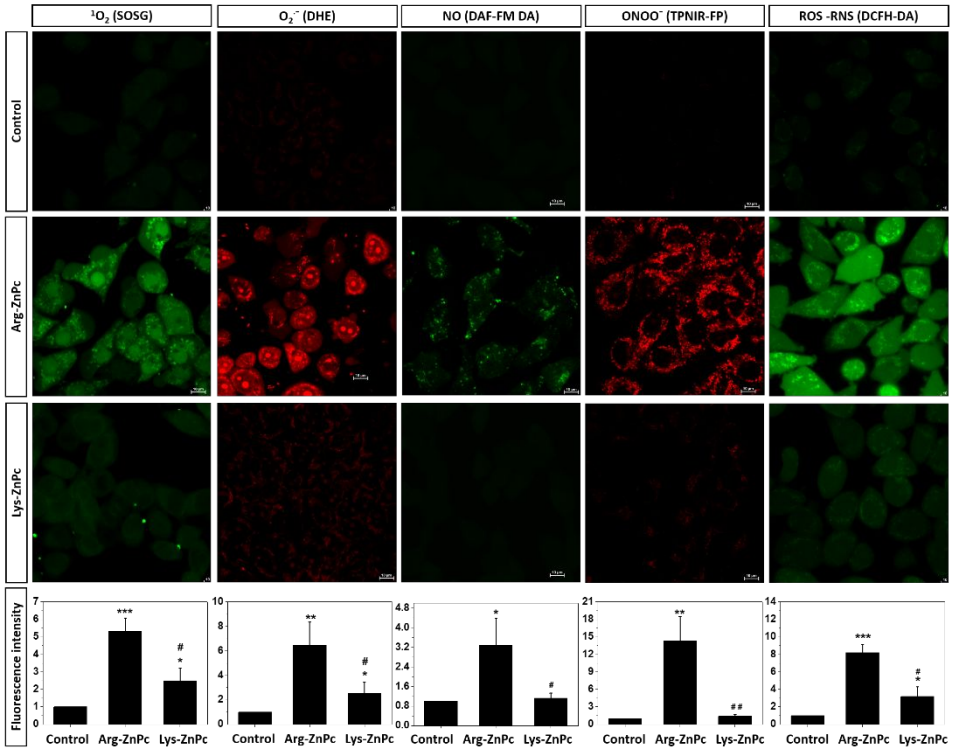

Figure 4. Fluorescence images and intensity comparison of intracellular $^1O_2$, $O_2^{\cdot-}$, NO, $ONOO^-$ and total ROS+RNS were detected by SOSG, DHE, DAF-FM DA, TPNIR-FP and DCFH-DA probes (Bar = 10 μm).

GSH Depletion Function. GSH is an important antioxidant defense of cells and its concentration in cancer cells is much higher than that in normal cells. ROS, NO and GSH are mutual constraints. GSH could consume ROS to reduce PDT efficiency. Similarly, GSH is also responsible for detoxifying NO-mediated cell damage. [32, 51] In turn, GSH could be depleted by ROS and NO through oxidation or nitrosation mechanism. [12] And GSH depletion could promote ROS oxidative damage efficiency and NO induced toxicity to enhance PDT and NO gas treatment effect. Thus, during repeated in vivo treatment, the front therapy induced GSH depletion could be helpful for subsequent PDT and NO combination treatment, which could obtain satisfied tumor suppression effect finally. Intracellular GSH depletion by the two ZnPcs were studied by GSH assay kit and GSH fluorescence probe. [52] After light irradiation, comparing with Lys-ZnPc, GSH depletion degree by Arg-ZnPc was aggravated possibly due to the combination contribution from ROS and NO (Figure 5 and Figure S16).

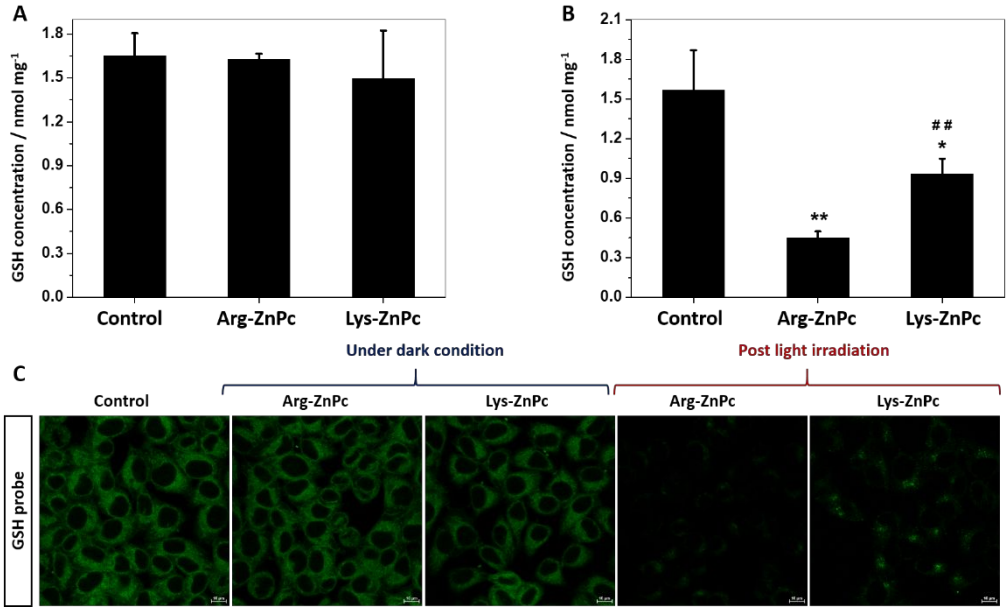

Figure 5. (A) Intracellular GSH concentration change in Arg-ZnPc or Lys-ZnPc treated cells before (A) and after (B) light irradiation from the detection results by GSH and GSSG assay kit; (C) intracellular GSH probe fluorescence intensity change in Arg-ZnPc or Lys-ZnPc treated cells before and after light irradiation (Bar = 10 μm).

P-gp Inhibition by NO to Avoid Drug Efflux. P-gp, a cell membrane protein, contributing to the development of drug resistance in cancer by promoting drug efflux, which could induce intracellular drug concentration decreasing to reduce activity. Reports indicated that NO can inhibit the P-gp expression at ultra-low concentration. [53] Thus, we proposed that Arg-ZnPc also has the P-gp expression inhibition function post NO release to avoid ZnPc efflux. The P-gp expression in cancer cells and tumor tissue were effectively inhibited in Arg-ZnPc treated group, which could be helpful for drug retention inside cancer cells. On the contrary, no obvious P-gp expression changing was detected in control and Lys-ZnPc treated group (Figure 6A and 6B), verifying P-gp expression was inhibited by NO.

To verify P-gp inhibition could avoid ZnPc efflux, cellular uptake effect of Arg-ZnPc or Lys-ZnPc was studied and compared with the function of prolonged incubation time. As shown in Figure 6C and Figure S17-S18, the cellular uptake percent of the two ZnPc were gradually increased from 8 to 48 h. After 48 h, obviously drug efflux could be detected. However, the drug

efflux effect of Arg-ZnPc was lower than Lys-ZnPc. These results indicated that P-gp down-regulation by NO could inhibit drug efflux, which could helpful for the enhanced PDT activity.

The drug efflux experiments were carried out in the dark. There was intrinsic ROS in cancer cells. Arginine modified compound can respond to intrinsic ROS to generate NO (Figure S19). [54] However, the amount was not enough for directly killing cancer cells since Arg-ZnPc was not induced effective cell death without light irradiation under our experiment condition ([Arg-ZnPc] = 2 μM). But, under such condition, P-gp down-regulation can be detected.

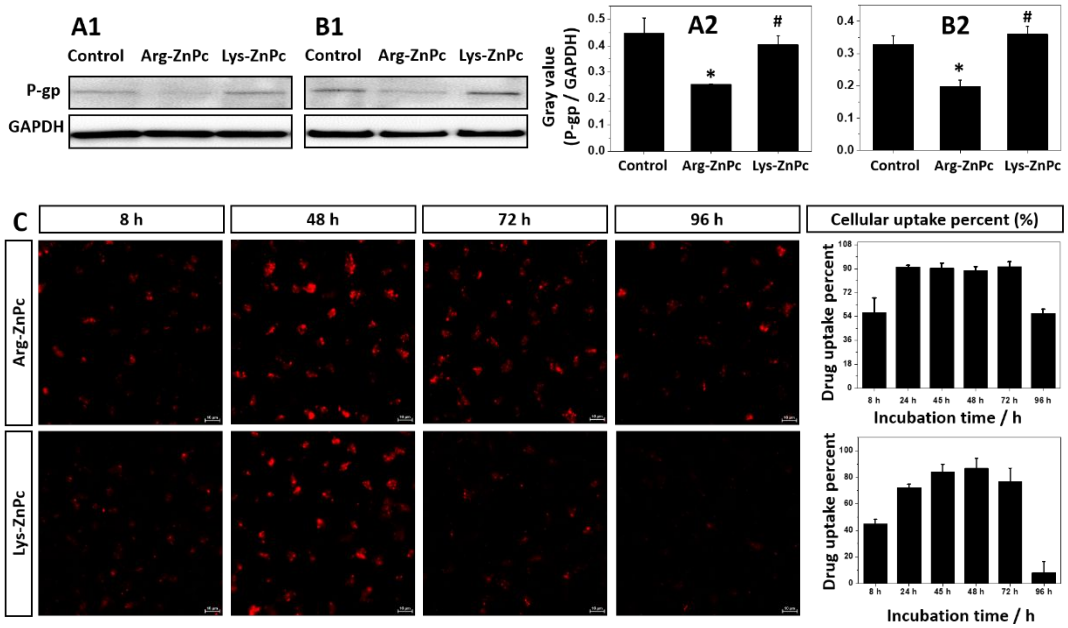

Figure 6. Western blot (A1) and quantitative analysis (A2) for the detection of P-gp expression in cancer cells post various drugs and light irradiation; western blot (B1) and quantitative analysis (B2) for the detection of P-gp expression in tumor tissue post various treatment; (C) detection of drug efflux effect with the prolonged incubation time (Bar = 10 μm).

Relaxation of Blood Vessel to Promote Drug Accumulation at Tumor. NO could promote tumor vasodilatation to enhance blood vessel permeability, and therefore promote drug (including nano-sized and molecular medicine) extravasation at tumor tissue. [55] To verify above hypothesis, the influence of NO from Arg-ZnPc on vascular permeability was studied in mouse dorsal skin model and subcutaneous transplantation tumor model. Evans blue assay is a classic method to measure vascular permeability. The subcutaneous injection of Arg-ZnPc at

dorsal skin of mice and light irradiation induced obvious evans blue leaking around the injection position (Figure 7A and 7B). On the contrary, evans blue leaking increasing in Lys-ZnPc treated one was weak. Similar results were obtained in subcutaneous transplantation tumor model. Obvious evans blue extravasation could be observed in Arg-ZnPc and light treated (at tumor position) post tail vein injection comparing with Lys-ZnPc or control group (Figure 7C and 7D). The results suggested that NO release from Arg-ZnPc could enhance tumor vascular permeability and improve the extravasation at tumor tissue.

In order to confirm the enhanced drug extravasation at tumor by NO, in vivo distribution of Arg-ZnPc and Lys-ZnPc was studied and compared. As shown in Figure 7E and 7F, tumor accumulation ability of Arg-ZnPc was obviously superior to Lys-ZnPc. In addition, a recent research indicated that the isomers of some phthalocyanines could have different pharmacokinetic property in a patient. [56] And we proposed such property would influence distribution of various ZnPc isomers.

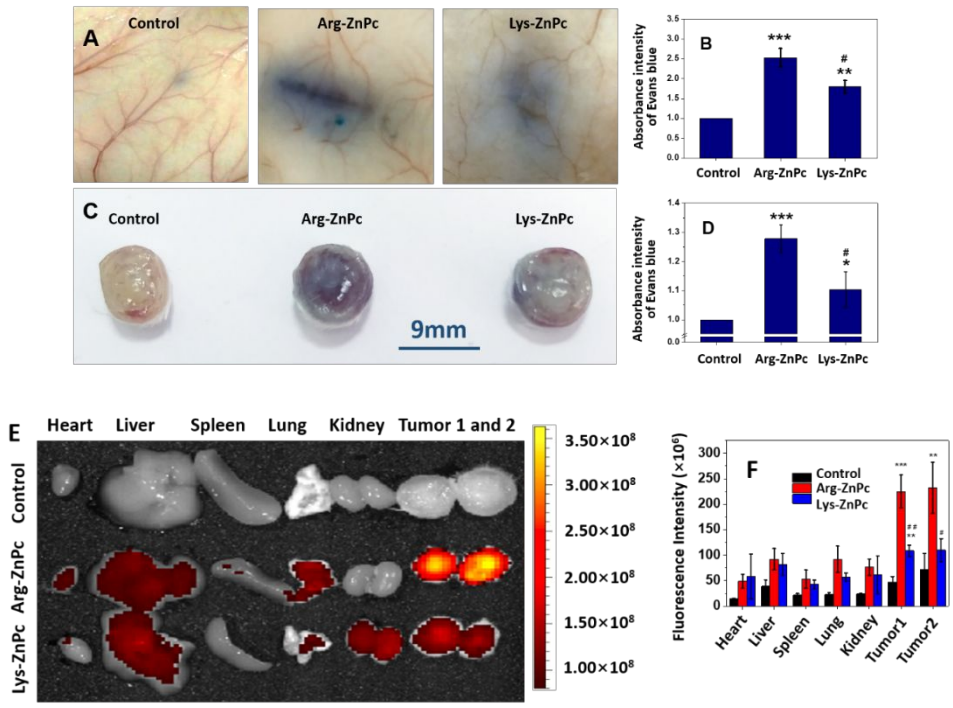

Figure 7. Experiments in skin (A) and tumor (C) for illustrating the enhanced vascular permeability effect using the evans blue assay; the quantification of the evans blue extravasation by methanamide from skin (B) and tumor (D); (E) in vivo imaging of tumor bearing mice after intravenous injection of saline, Arg-ZnPc and Lys-ZnPc post 3 days treatment and

the mean fluorescence intensity of their major organs and tumor (F).

PDT, a FDA approved cancer treatment modality, utilizes non-toxic PS, light and O_2 to generate cytotoxic ROS to kills cancer cells. Gas therapy uses various gases to influence diverse physiological and pathophysiological processes for disease treatment. Many researches indicated that the combination of gas therapy and other traditional cancer therapy modality was an effective way to obtain satisfied cancer treatment outcome. However, combination of NO and PDT could obtain positive or negative effect for cancer treatment since NO can play either pro-survival or pro-death roles in PDT. Reports indicated that the high biocidal $ONOO^-$ formation efficiency by NO and $O_2^{\bullet -}$ determined the synergistic treatment outcome. And the distance between NO and $O_2^{\bullet -}$ can decide $ONOO^-$ generation performance. Thus, here, an arginine modified ZnPc was designed and synthesized as bifunctional drug (photosensitizer and NO donor) and a lysine modified ZnPc was synthesized as a control drug. PDT process generates various ROS, including $O_2^{\bullet -}$, efficiently. Simultaneously, the ROS can oxidize guanido of Arg-ZnPc to release NO. NO and $O_2^{\bullet -}$ generation at the same place and time can ensure effective $ONOO^-$ formation. Furthermore, NO can promote tumor vasodilatation and down-regulate cancer cells P-gp expression to enhance drug extravasation and retention at tumor tissue. NO also can deplete reduced GSH inside cancer cells to avoid its ROS consuming. These synergistic functions of NO further improve PDT treatment activity. In vitro and in vivo results all indicated that the anticancer activity of Arg-ZnPc was superior to Lys-ZnPc. Thus, integrating ROS response NO donor within PS was an ideal strategy to utilize NO for gas therapy and PDT combination for cancer treatment.

ASSOCIATED CONTENT

Supporting Information.

The Supporting Information is available free of charge on the ACS Publications website.

Supplemental data including materials and instrumentation, MS-MALDI-TOF spectrometer, molar extinction coefficients and UV-Vis spectra, dark toxicity, fluorescent images and intensity, uptake percent and references.

ACKNOWLEDGEMENTS

This work was supported by the National Natural Science Foundation of China (grant number 21671105), the project (grant number BK20161554) supported by NSF of Jiangsu Province of China, the Priority Academic Program Development of Jiangsu Higher Education Institutions and the Foundation of Jiangsu Collaborative Innovation Centre of Biomedical Functional Materials (grant number 161090H001), the New Technologies and Methods of Scientific Instrument and Equipment Sharing Service Platform in Jiangsu province and the Postgraduate innovation Project of Jiangsu Province (grant number 1812000006477).

ABBREVIATIONS: NO, nitric oxide; PDT, photodynamic therapy; $ONOO^-$, oxidizing peroxynitrite anions; $O_2^{\bullet -}$, superoxide anions; Arg, L-arginine; ZnPc, zinc phthalocyanine; Arg-ZnPc, L-arginine ethyl ester modified ZnPc; ROS, reactive oxygen species; P-gp, P-glycoprotein; GSH, reduced glutathione; PS, photosensitizers; $^1O_2$, singlet oxygen; $HO^{\bullet}$, hydroxyl radicals; H_2O_2, hydrogen peroxide; RNS, reactive nitrogen species; Lys-ZnPc, L-lysine ethyl ester linked ZnPc; TPNIR-FP, two-photon-excitable and NIR-emissive fluorescence probe; DBU, 1, 8-diazabicyclo [5, 4, 0]-undec-7-ene; DMSO, dimethyl sulfoxide; EDC·HCl, 1-(3-Dimethylaminopropyl)-3-ethylcarbodiimide hydrochloride; HOBt, 1-Hydroxybenzotriazole; DMF, N, N-dimethyl-formamide; DIPEA N, N-Diisopropylethylamine; TPNIR-NH_2, two-photon-excitable and NIR-emissive amidogen; DMEM, dulbecco's modified eagle media; FBS, fetal bovine serum; MTT, 3-[4, 5-dimethylthiazol-2-yl]-2, 5-diphenyl tetrazolium bromide; LED, light emitting diode; FCM, flow cytometry; CLSM, confocal laser scanning microscope; ADPA, 9, 10-anthracenedip-ropionic acid; DHE, dihydroethidium; DAF-FM DA, 3-Amino, 4-aminomethyl-2′, 7′-difluorescein, diacetate; SOSG, singlet oxygen sensor green reagent; DCFH-DA, 2, 7-dichlorofluorescin diacetate; c-PTIO, carboxy-PTIO; GSSG, oxidized glutathione; RIPA, radio immune precipitation assay; TBST, Tris-HCl buffer saline and tween; GAPDH, glyceraldehyde-3-phosphate dehydrogenase; ECL, enhanced chemiluminescence; H&E, hematoxylin & eosin.

REFERENCES

1. Li, X.; Lee, S.; Yoon, J. Supramolecular photosensitizers rejuvenate photodynamic therapy. *Chem. Soc. Rev.* **2018,** *47*, 1174-1188.

2. Agostinis, P.; Berg, K.; Cengel, K. A.; Foster, T. H.; Girotti, A. W.; Gollnick, S. O.; Hahn,

S. M.; Hamblin, M. R.; Juzeniene, A.; Kessel, D.; Korbelik, M.; Moan, J.; Mroz, P.; Nowis, D.; Piette, J.; Wilson, B. C.; Golab, J. Photodynamic therapy of cancer: an update. *CA Cancer J. Clin.* **2011,** *61*, 250-281.

3. Fan, W.; Yung, B. C.; Chen, X. Stimuli-responsive NO release for on-demand gas-sensitized synergistic cancer therapy. *Angew. Chem. Int. Ed.* **2018,** *57*, 8383-8394.

4. Wang, C.; Li, Y.; Shi, X.; Zhou, J.; Zhou, L.; Wei, S. Use of an NIR-light-responsive CO nanodonor to improve the EPR effect in photothermal cancer treatment. *Chem. Commun.* **2018,** *54*, 13403-13406.

5. Li, S.; Liu, R.; Jiang, X.; Qiu, Y.; Song, X.; Huang, G.; Fu, N.; Lin, L.; Song, J.; Chen, X.; Yang, H. Near-infrared light-triggered sulfur dioxide gas therapy of cancer. *ACS Nano* **2019,** *13*, 2103-2113.

6. Kang, J.; Li, Z.; Organ, C. L.; Park, C. M.; Yang, C. T.; Pacheco, A.; Wang, D.; Lefer, D. J.; Xian, M. pH-Controlled hydrogen sulfide release for myocardial ischemia-reperfusion injury. *J. Am. Chem. Soc.* **2016,** *138*, 6336-6339.

7. Huang, X.; Xu, F.; Hou, H.; Hou, J.; Wang, Y.; Zhou, S. Stimuli-responsive nitric oxide generator for light-triggered synergistic cancer photothermal/gas therapy. *Nano Res.* **2019,** *12*, 1361-1370.

8. Yu, L.; Hu, P.; Chen, Y. Gas-generating nanoplatforms: material chemistry, multifunctionality, and gas therapy. *Adv. Mater.* **2018,** *30*, DOI: 1801964.

9. Zhang, X.; Tian, G.; Yin, W.; Wang, L.; Zheng, X.; Yan, L.; Li, J.; Su, H.; Chen, C.; Gu, Z.; Zhao, Y. Controllable generation of nitric oxide by near-infrared-sensitized upconversion nanoparticles for tumor therapy. *Adv. Funct. Mater.* **2015,** *25*, 3049-3056.

10. Wu, J.; Akaike, T.; Hayashida, K.; Okamoto, T.; Okuyama, A.; Maeda, H. Enhanced vascular permeability in solid tumor involving peroxynitrite and matrix metalloproteinases. *Jpn. J. Cancer Res.* **2001,** *92*, 439-451.

11. Maeda, H.; Wu, J.; Sawa, T.; Matsumura, Y.; Hori, K. Tumor vascular permeability and the EPR effect in macromolecular therapeutics: a review. *J Control. Release* **2000,** *65*, 271-284.

12. Jourd'heuil, D.; Jourd'heuil, F. L.; Feelisch, M. Oxidation and nitrosation of thiols at low micromolar exposure to nitric oxide. Evidence for a free radical mechanism. *J. Biol. Chem.* **2003,** *278*, 15720-15726.

13. Fahey, J. M.; Girotti, A. W. Nitric oxide-mediated resistance to photodynamic therapy in a human breast tumor xenograft model: improved outcome with NOS2 inhibitors. *Nitric Oxide* **2017,** *62*, 52-61.

14. Girotti, A. W. Modulation of the anti-tumor efficacy of photodynamic therapy by nitric oxide. *Cancers* **2016,** *8*, DOI: 10.3390/cancers8100096.

15. Bhowmick, R.; Girotti, A. W. Pro-survival and pro-growth effects of stress-induced nitric oxide in a prostate cancer photodynamic therapy model. *Cancer Lett.* **2014,** *343*, 115-122.

16. Bhowmick, R.; Girotti, A. W. Cytoprotective signaling associated with nitric oxide upregulation in tumor cells subjected to photodynamic therapy-like oxidative stress. *Free Radic. Biol. Med.* **2013,** *57*, 39-48.

17. Xiang, H. J.; Deng, Q.; An, L.; Guo, M.; Yang, S. P.; Liu, J. G. Tumor cell specific and lysosome-targeted delivery of nitric oxide for enhanced photodynamic therapy triggered by 808 nm near-infrared light. *Chem. Commun.* **2016,** *52*, 148-151.

18. Deng, Y.; Jia, F.; Chen, S.; Shen, Z.; Jin, Q.; Fu, G.; Ji, J. Nitric oxide as an all-rounder for enhanced photodynamic therapy: hypoxia relief, glutathione depletion and reactive nitrogen species generation. *Biomaterials* **2018,** *187*, 55-65.

19. Rapozzi, V.; Della Pietra, E.; Zorzet, S.; Zacchigna, M.; Bonavida, B.; Xodo, L. E. Nitric oxide-mediated activity in anti-cancer photodynamic therapy. *Nitric Oxide* **2013,** *30*, 26-35.

20. Rapozzi, V.; Della Pietra, E.; Bonavida, B. Dual roles of nitric oxide in the regulation of tumor cell response and resistance to photodynamic therapy. *Redox Biol.* **2015,** *6*, 311-317.

21. Wink, D. A.; Mitchell, J. B. Chemical biology of nitric oxide: insights into regulatory, cytotoxic, and cytoprotective mechanisms of nitric oxide. *Free Radic. Biol. Med.* **1998,** *25*, 434-456.

22. Beckman, J. S.; Carson, M.; Smith, C. D.; Koppenol, W. H. ALS, SOD and peroxynitrite. *Nature* **1993,** *364*, 584-584.

23. Deepagan, V. G.; Ko, H.; Kwon, S.; Rao, N. V.; Kim, S. K.; Um, W.; Lee, S.; Min, J.; Lee, J.; Choi, K. Y.; Shin, S.; Suh, M.; Park, J. H. Intracellularly activatable nanovasodilators to enhance passive cancer targeting regime. *Nano Lett.* **2018,** *18*, 2637-2644.

24. Quinn, J. F.; Whittaker, M. R.; Davis, T. P. Delivering nitric oxide with nanoparticles. *J. Control. Release* **2015,** *205*, 190-205.

25. Chandrawati, R.; Chang, J. Y. H.; Reina-Torres, E.; Jumeaux, C.; Sherwood, J. M.; Stamer, W. D.; Zelikin, A. N.; Overby, D. R.; Stevens, M. M. Localized and controlled delivery of nitric oxide to the conventional outflow pathway via enzyme biocatalysis: toward therapy for glaucoma. *Adv. Mater.* **2017,** *29*, DOI: 10.1002/adma.201604932.

26. Jin, H.; Yang, L.; Ahonen, M. J. R.; Schoenfisch, M. H. Nitric oxide-releasing cyclodextrins. *J. Am. Chem. Soc.* **2018,** *140*, 14178-14184.

27. Hou, J.; Pan, Y.; Zhu, D.; Fan, Y.; Feng, G.; Wei, Y.; Wang, H.; Qin, K.; Zhao, T.; Yang, Q.; Zhu, Y.; Che, Y.; Liu, Y.; Cheng, J.; Kong, D.; Wang, P. G.; Shen, J.; Zhao, Q. Targeted delivery of nitric oxide via a 'bump-and-hole'-based enzyme-prodrug pair. *Nat. Chem. Biol.* **2019,** *15*, 151-160.

28. Fan, W.; Lu, N.; Huang, P.; Liu, Y.; Yang, Z.; Wang, S.; Yu, G.; Liu, Y.; Hu, J.; He, Q.; Qu, J.; Wang, T.; Chen, X. Glucose-responsive sequential generation of hydrogen peroxide and nitric oxide for synergistic cancer starving-like/gas therapy. *Angew. Chem. Int. Ed.* **2017,** *56*, 1229-1233.

29. Birben, E.; Sahiner, U. M.; Sackesen, C.; Erzurum, S.; Kalayci, O. Oxidative stress and antioxidant defense. *World Allergy Organ. J.* **2012,** *5*, 9-19.

30. Russo, A.; DeGraff, W.; Friedman, N.; Mitchell, J. B. Selective modulation of glutathione levels in human normal versus tumor cells and subsequent differential response to chemotherapy drugs. *Cancer Res.* **1986,** *46*, 2845-2848.

31. Zhang, W.; Lu, J.; Gao, X.; Li, P.; Zhang, W.; Ma, Y.; Wang, H.; Tang, B. Enhanced photodynamic therapy by reduced levels of intracellular glutathione obtained by employing a nano-MOF with Cu(II) as the active center. *Angew. Chem. Int. Ed.* **2018,** *57*, 4891-4896.

32. Ju, E.; Dong, K.; Chen, Z.; Liu, Z.; Liu, C.; Huang, Y.; Wang, Z.; Pu, F.; Ren, J.; Qu, X. Copper(II)-graphitic carbon nitride triggered synergy: improved ROS generation and reduced glutathione levels for enhanced photodynamic therapy. *Angew. Chem. Int. Ed.* **2016,** *128*, 11639-11643.

33. Wang, A.; Zhou, R.; Zhou, L.; Sun, K.; Zhou, J.; Wei, S.; Jiang, J. Arginine-substituted phthalocyanine with concentration-driven self-disaggregation performance: synthesis, properties and mechanistic study. *Chem. Asian J.* **2016,** *11*, 3008-3013.

34. Shang, H.; Chen, H.; Tang, Y.; Ma, Y.; Lin, W. Development of a two-photon fluorescent

turn-on probe with far-red emission for thiophenols and its bioimaging application in living tissues. *Biosens Bioelectron* **2017,** *95*, 81-86.

35. Xie, X.; Tang, F.; Liu, G.; Li, Y.; Su, X.; Jiao, X.; Wang, X.; Tang, B. Mitochondrial peroxynitrite mediation of anthracycline-induced cardiotoxicity as visualized by a two-photon near-infrared fluorescent probe. *Anal. Chem.* **2018,** *90*, 11629-11635.

36. Sarı, S.; Durmuş, M.; Bulut, M. Microwave assisted synthesis of novel zinc(II) phthalocyanines bearing 1,3-diazido-2-propanoxy functional groups and investigation of their photochemical properties. *Tetrahedron Lett.* **2016,** *57*, 1124-1128.

37. Nyokong, T. Effects of substituents on the photochemical and photophysical properties of main group metal phthalocyanines. *Coordin. Chem. Rev.* **2007,** *251*, 1707-1722.

38. Li, X. S.; Ke, M. R.; Zhang, M. F.; Tang, Q. Q.; Zheng, B. Y.; Huang, J. D. A non-aggregated and tumour-associated macrophage-targeted photosensitiser for photodynamic therapy: a novel zinc(II) phthalocyanine containing octa-sulphonates. *Chem. Commun.* **2015,** *51*, 4704-4707.

39. Li, X.; Peng, X. H.; Zheng, B. D.; Tang, J.; Zhao, Y.; Zheng, B. Y.; Ke, M. R.; Huang, J. D. New application of phthalocyanine molecules: from photodynamic therapy to photothermal therapy by means of structural regulation rather than formation of aggregates. *Chem. Sci.* **2018,** *9*, 2098-2104.

40. Zorlu, Y.; Ermeydan, M. A.; Dumoulin, F.; Ahsen, V.; Savoie, H.; Boyle, R. W. Glycerol and galactose substituted zinc phthalocyanines. Synthesis and photodynamic activity. *Photochem. Photobiol. Sci.* **2009,** *8*, 312-318.

41. Crowley, L. C.; Marfell, B. J.; Scott, A. P.; Waterhouse, N. J. Quantitation of apoptosis and necrosis by annexin V binding, propidium iodide uptake, and flow cytometry. *Cold Spring Harb. Protoc.* **2016,** DOI: 10.1101/pdb.prot087288.

42. Lukinavicius, G.; Blaukopf, C.; Pershagen, E.; Schena, A.; Reymond, L.; Derivery, E.; Gonzalez-Gaitan, M.; D'Este, E.; Hell, S. W.; Wolfram Gerlich, D.; Johnsson, K. SiR-hoechst is a far-red DNA stain for live-cell nanoscopy. *Nat. Commun.* **2015,** *6*, 8497-8503.

43. Fischer, A. H.; Jacobson, K. A.; Rose, J.; Zeller, R. Cutting sections of paraffin-embedded tissues. *CSH Protoc.* **2008,** DOI: 10.1101/pdb prot4987.

44. Duong, H. T.; Kamarudin, Z. M.; Erlich, R. B.; Li, Y.; Jones, M. W.; Kavallaris, M.; Boyer,

C.; Davis, T. P. Intracellular nitric oxide delivery from stable NO-polymeric nanoparticle carriers. *Chem. Commun.* **2013,** *49*, 4190-4192.

45. Li, X.; Zheng, B.-D.; Peng, X.-H.; Li, S.-Z.; Ying, J.-W.; Zhao, Y.; Huang, J.-D.; Yoon, J. Phthalocyanines as medicinal photosensitizers: developments in the last five years. *Coordin. Chem. Rev.* **2019,** *379*, 147-160.

46. Zhang, X.-F.; Zheng, H. Tetra(β-phenothiazinyl) zinc phthalocyanine: An easily prepared D4–A system for efficient photoinduced electron transfer. *Inorg. Chim. Acta* **2010,** *363*, 2259-2264.

47. George, R. D.; Snow, A. W.; Shirk, J. S.; Barger, W. R. The alpha substitution effect on phthalocyanine aggregation. *J. Porphyr. Phthalocya.* **1998,** *2*, 1-7.

48. Ngubeni, G. N.; Britton, J.; Mack, J.; New, E.; Hancox, I.; Walker, M.; Nyokong, T.; Jones, T. S.; Khene, S. Spectroscopic and nonlinear optical properties of the four positional isomers of 4α-(4-tert-butylphenoxy)phthalocyanine. *J. Mater. Chem. C* **2015,** *3*, 10705-10714.

49. Chen, Y.; Fang, W.; Wang, K.; Liu, W.; Jiang, J. Nonperipheral tetrakis(dibutylamino)phthalocyanines. new types of 1,8,15,22-tetrakis(substituted)phthalocyanine isomers. *Inorg. Chem.* **2016,** *55*, 9289-9296.

50. Rastogi, R. P.; Singh, S. P.; Häder, D.-P.; Sinha, R. P. Detection of reactive oxygen species (ROS) by the oxidant-sensing probe 2′,7′-dichlorodihydrofluorescein diacetate in the cyanobacterium anabaena variabilis PCC 7937. *Biochem. Bioph. Res. Commun.* **2010,** *397*, 603-607.

51. Yin, S. Y.; Song, G.; Yang, Y.; Zhao, Y.; Wang, P.; Zhu, L. M.; Yin, X.; Zhang, X. B. Persistent regulation of tumor microenvironment via circulating catalysis of $MnFe_2O_4$@metal–organic frameworks for enhanced photodynamic therapy. *Adv. Funct. Mater.* **2019**, DOI: 10.1002/adfm.201901417.

52. Zhang, Q.; Yu, D.; Ding, S.; Feng, G. A low dose, highly selective and sensitive colorimetric and fluorescent probe for biothiols and its application in bioimaging. *Chem. Commun.* **2014,** *50*, 14002-14005.

53. Guo, R.; Tian, Y.; Wang, Y.; Yang, W. Near-infrared laser-triggered nitric oxide nanogenerators for the reversal of multidrug resistance in cancer. *Adv. Funct. Mater.* **2017,** *27*, DOI: 10.1002/adfm.201606398.

54. Wan, M.; Chen, H.; Wang, Q.; Niu, Q.; Xu, P.; Yu, Y.; Zhu, T.; Mao, C.; Shen, J. Bio-inspired nitric-oxide-driven nanomotor. *Nat. Commun.* **2019,** *10*, DOI: 10.1038/s41467.

55. Fang, J.; Nakamura, H.; Maeda, H. The EPR effect: unique features of tumor blood vessels for drug delivery, factors involved, and limitations and augmentation of the effect. *Adv. Drug Deliv. Rev.* **2011,** *63*, 136-151.

56. Zheng, X.; Cui, X.; Yu, H.; Jiang, J. Development of a quantitative method for four photocyanine isomers using differential ion mobility and tandem mass spectrometry and its application in a preliminary pharmacokinetics investigation. *J. Chromatogr. A* **2018,** *1577*, 109-119.

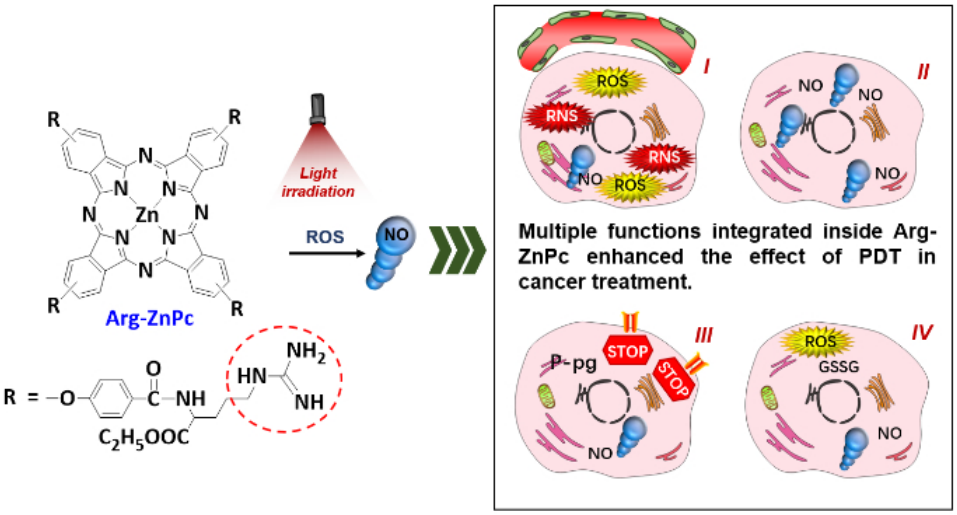

Mechanism diagram of multiple functions integrated inside Arg-ZnPc for its PDT activity amplification

82x44mm (220 x 220 DPI)